

Polymeric “Clickase” Accelerates the Copper Click Reaction of Small Molecules, Proteins, and Cells

Junfeng Chen,[†] Jiang Wang,[‡] Ke Li,[†] Yuhan Wang,[§] Martin Gruebele,^{†,‡,§} Andrew L. Ferguson,[¶] and Steven C. Zimmerman^{*,†,§}

[†]Department of Chemistry, University of Illinois, Urbana, Illinois 61801, United States.

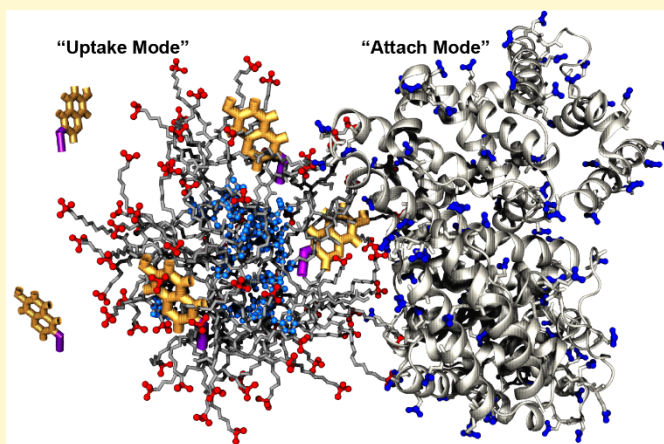
[‡]Department of Physics, University of Illinois, Urbana, Illinois 61801, United States.

[§]Center for Biophysics and Quantitative Biology, University of Illinois, Urbana, Illinois 61801, United States.

[¶]Institute for Molecular Engineering, The University of Chicago, Chicago, Illinois 60637, United States.

Supporting Information

ABSTRACT: Recent work has shown that polymeric catalysts can mimic some of the remarkable features of metalloenzymes by binding substrates in proximity to a bound metal center. We report here an unexpected role for the polymer: multivalent, reversible, and adaptive binding to protein surfaces allowing for accelerated catalytic modification of proteins. The catalysts studied are a group of copper-containing single-chain polymeric nanoparticles (Cu^I-SCNP) that exhibit enzyme-like catalysis of the copper-mediated azide-alkyne cycloaddition reaction. The Cu^I-SCNP use a previously observed “uptake mode,” binding small molecule alkynes and azides inside a water-soluble amphiphilic polymer and proximal to copper catalytic sites, but with unprecedented rates. Remarkably, a combined experimental and computational study shows that the same Cu^I-SCNP perform a more efficient click reaction on modified protein surfaces and cell surface glycans than do small molecule catalysts. The catalysis occurs through an “attach mode” where the SCNP reversibly binds protein surfaces through multiple hydrophobic and electrostatic contacts. The results more broadly point to a wider capability for polymeric catalysts as artificial metalloenzymes, especially as it relates to bio-applications.



■ INTRODUCTION

Synthetic transition metal catalysts are able to perform reactions in buffered solution, *in cellulo*, and even *in vivo*. As such, these catalysts are important tools for chemical biology and potentially as new therapeutic agents,¹⁻³ with recent applications ranging from bio-conjugation reactions⁴ and cell surface editing⁵ to *in situ* drug synthesis.⁶ Many of the metal catalysts used were optimized for organic synthesis and, thus, function best in aprotic solvents and with reagent concentrations in the 0.1-1 M range. In competitive biological media and at the low substrate concentrations frequently used in bioapplications, the same catalysts often function poorly. Transition metal catalysis is common in biology with nature managing these same challenges through the use of metalloenzymes. In particular, the precisely folded polypeptide scaffolds function to protect the metal center and create a binding cavity to bring the substrate and metal together.

Considerable recent effort has focused on artificial metallo-enzymes that combine non-natural transition metal catalysts with either proteins^{7,8} or polymeric scaffolds.^{9,10} The surrounding protein or polymer serves as a functional

surrogate for the metalloenzyme polypeptide backbone. Among the efforts to develop polymeric transition metal catalysts, single chain nanoparticles (SCNPs) have emerged as an especially promising approach.¹¹⁻¹³ The advantages of SCNPs include their modular synthesis,¹⁴ broad range of cross-linking chemistries,¹¹ adjustable size,¹⁴ tunable cell uptake,¹⁵ SCNP based catalysts have been reported to conduct reactions in aqueous buffer and inside cells,^{16,17} and accelerate reactions by binding the substrates supramolecularly, the latter demonstrating their artificial metalloenzyme behavior.^{18,19}

We focused on SCNP-based catalysts for the copper-mediated alkyne-azide cycloaddition (CuAAC) “click” reaction, because it is arguably the most important (bio)orthogonal conjugation reaction,²⁰ yet still limited by copper toxicity and the need for low concentrations in biological applications.^{21,22} We previously used water-soluble amphiphilic ROMP-derived polymers containing amino acid side-chains for Cu^I binding. These copper-based SCNP (Cu^I-SCNP-1) functioned as “clickases,” showing enzyme-like click catalysis and giving serviceable rates at micromolar substrate concentrations and part-per-million

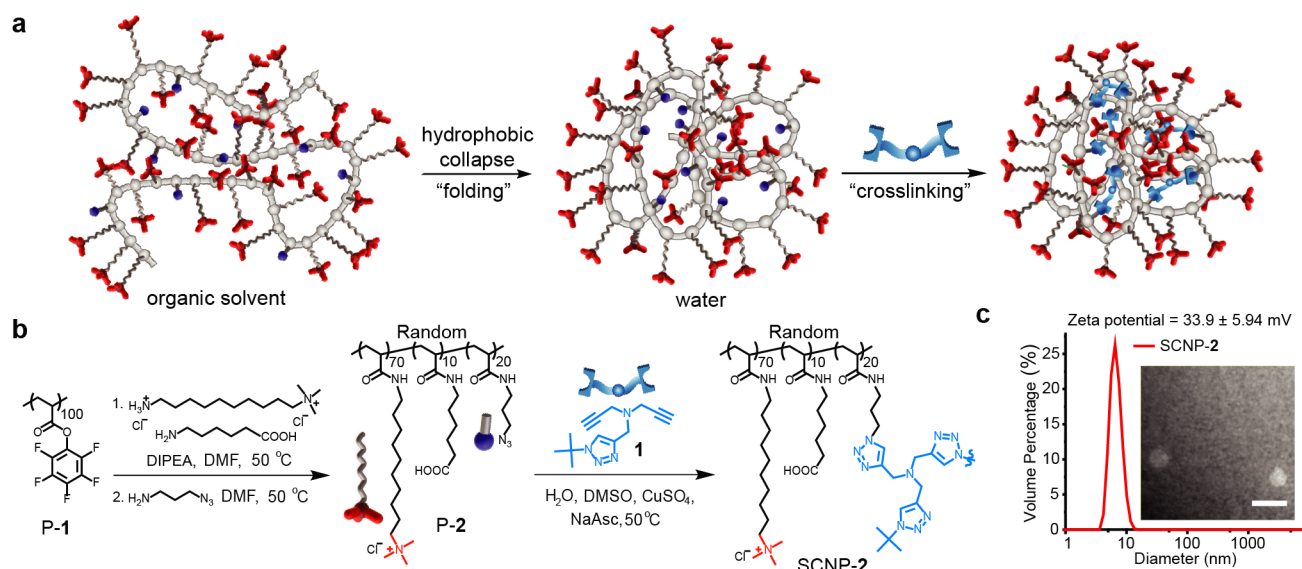


Figure 1. SCNP preparation. (a) Illustration of SCNP preparation using a “folding and crosslinking” strategy wherein hydrophobic collapse and electrostatic repulsion of unimolecular micelle-like structures allows higher concentration crosslinking. (b) Two-step conversion of P-1 to SCNP-2. c, DLS data and TEM image (inset) of SCNP-2. Scale bar = 20 nm.

levels of copper.^{16,18} Herein we report a new class of polyacrylamide-based SCNP (SCNP-2) that catalyze the CuAAC click reaction with rates significantly faster than SCNP-1 and the best available tris(triazolylmethyl)amine ligands. More strikingly, we report the unexpected discovery that Cu^I-SCNP-2 adaptively and reversibly binds protein surfaces accelerating the click reaction of modified proteins and enabling efficient surface glycan editing.²³

RESULTS AND DISCUSSION

Synthesis of SCNPs through “folding and crosslinking” strategy. The development of SCNP-2 was enabled by three key innovations. The first involved changing from the poly(norbornene imide) backbone used in SCNP-1 to a polyacrylamide-based SCNP related to that reported by Meijer and Palmans.^{17,19} This change was motivated by the finding that the hydrophobic poly(norbornene imide) backbone did not appear to participate in substrate

binding.¹⁸ Second, we sought to overcome one of the major challenges of synthesizing SCNPs on scale, the need for high dilution cross-linking to minimize inter-chain coupling.²⁴ Third, a covalent cross-linking strategy was employed that installed a tris(triazolylmethyl)-amine unit to serve as a more effective Cu^I ligand (see below).

To increase the propensity for intrachain crosslinking, a “folding and crosslinking” strategy was pursued (Figure 1a). Thus, poly(pentafluorophenyl acrylate) (P-1) was prepared with DP = 95, M_n = 23 kDa, and PDI = 1.05 by RAFT polymerization.¹⁷ Successive treatment with (10-aminodecyl)trimethylammonium chloride and 6-aminohexanoic acid followed by 3-azidopropyl-amine provided polyacrylamide P-2. In water, P-2 likely undergoes hydrophobic collapse forming a unimolecular micelle-like structure. By using the hydrophobic crosslinker, diyne **1**, P-2 could be covalently crosslinked using the CuAAC reaction. The repulsion between polycationic

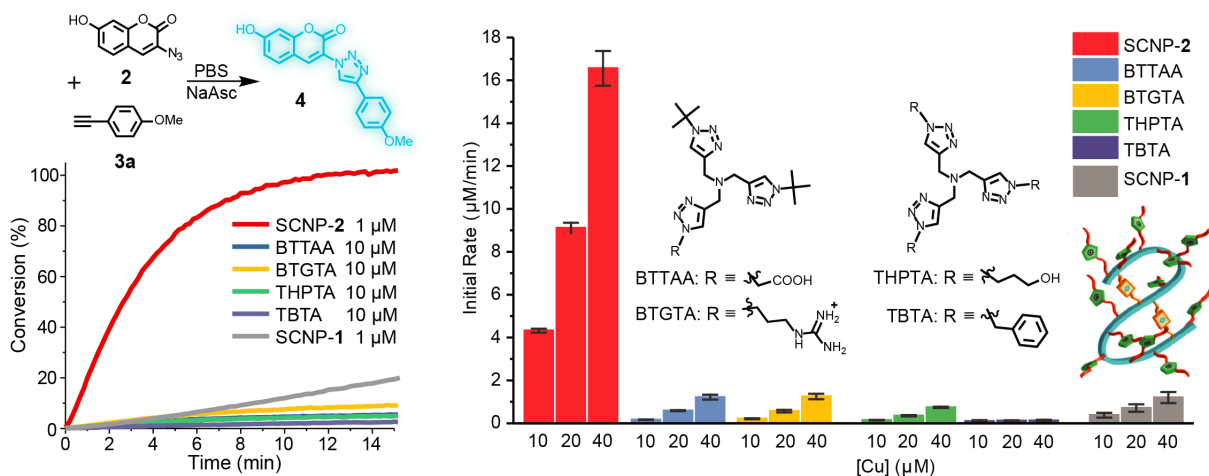


Figure 2. Comparison reactions conducted in PBS buffer (1x, pH = 7.4) at room temp with **2** (20 μM), **3a** (40 μM), sodium ascorbate (2 mM) and the catalyst. [SCNP-1] = [SCNP-2] = 1, 2, 4 μM (ave. 10 copper ions per SCNP). [BTTAA] = [BTGTA] = [THPTA] = [TBTA] = 10, 20, 40 μM. Throughout a 1:1 ratio of ligand and CuSO₄ used. The error bars for initial rates are the standard deviation of three independent experiments.

charges on P-2 inhibits aggregation and allows the crosslinking to occur intramolecularly at 0.2 mM a near 100-fold higher concentration than used for our previously reported covalent crosslinked SCNPs.¹⁴ The nanoparticles were imaged both by transmission electron microscopy (TEM) and atomic force microscopy (AFM) (Figure S2 and S3). The hydrodynamic diameter of SCNPs were determined to be around 6 nm using dynamic light scattering (DLS) and diffusion-ordered spectroscopy (DOSY) nuclear magnetic resonance (NMR). The shorter relaxation time T_2 measured by NMR indicated a more rigid structure after the crosslinking, supporting the crosslinked structure.

Uptake Mode: The CuAAC Click Reaction of Small Molecules. Inspired by the development of the BTAA ligand by Marlow, Liu, Wu, and coworkers,^{21,22} which is reported to give the fastest known CuAAC reaction, 6-aminohexanoic acid was used in the preparation of P-2 followed by the use of diyne **1** in the click-mediated covalent crosslinking reaction. Thus, SCNP-2 provides a polymeric scaffold surrounding the BTAA-like units. The SCNPs could be prepared with different degrees of crosslinking, but typically an average of ten crosslinks and thus ten copper binding sites per nanoparticle were used. To determine the catalytic performance of Cu^I-SCNP-2, the rate of the fluorogenic click reaction between azide **2** and alkyne **3a** was measured.²⁵ The rates were compared to those with SCNP-1, our previously reported SCNP¹⁶ and high-performance small molecule catalysts prepared from CuSO₄ and several tris(triazolyl-methyl)amine-based ligands, including TBTA,²⁶ THPTA,²⁶ and BTAA²² (Figure 2). Each reaction was performed at [CuSO₄] = 10, 20 and 40 μM and a 1:1 ligand-copper ratio and in the presence of sodium ascorbate as the reducing agent. Thus, the small molecule catalyst runs were at 10-fold higher catalyst concentration because each SCNP has on average ten copper binding sites.

Cu^I-SCNP-2 performs the CuAAC click reaction between **2** and **3a** significantly faster than the other catalysts. On average, its reaction rate is 10 times faster than the most efficient small molecule catalyst Cu^I-BTAA as well as Cu^I-SCNP-1 (Figure 2). A near quantitative conversion was observed within 10 min with only 10 μM of copper. To our knowledge, Cu^I-SCNP-2 is the most efficient catalyst reported to date for the “native” CuAAC reaction. The utility of Cu^I-SCNP-2 for typical synthetic reactions was also studied in water with several hydrophobic alkyne and azide substrates. Using 0.002 mol% of Cu^I-SCNP-2, the reactions gave isolated yields ranging from 92% to 98%, indicating high turnover numbers (Table S1). Because the amount of polymer and copper used is so small, we did not focus on recyclability. Nonetheless, after the fluorogenic reaction, Cu^I-SCNP-2 could be isolated following the click reaction of **2** and **3a** and a second round of catalysis showed a very similar kinetic profile (Figure S4).

The positively charged surface and hydrophobic interior provide Cu^I-SCNP-2 with the ability to bind substrates resulting in a high local concentration of substrates in proximity to the catalytic Cu^I centers (uptake mode).^{27,28} To probe the role of substrate charge and hydrophobicity, the rate of the CuAAC reaction between Cu^I-SCNP-2 and alkynes **3** and **5-7** were measured. These 14 alkynes can be assigned to four groups: neutral aromatic alkynes (**3**) and cationic (**5**), neutral (**6**), and anionic (**7**) aliphatic alkynes (Figure 3a). Cu^I-SCNP-2 showed high CuAAC activity for all substrates except the low molecular weight cationic alkynes

5a-c (Figure 3b). The fastest rates are seen with the more hydrophobic substrates, although the high activity of Cu^I-SCNP-2 means that the rate differences between substrates are much smaller than those observed with Cu^I-SCNP-1 (Figure S6). The macromolecular architecture of Cu^I-SCNP-2 conferred an average rate acceleration of 18-fold relative to the most efficient small molecule catalyst Cu^I-BTAA for the same reaction.

Molecular dynamics (MD) simulations of SCNP-2 in a water box were performed for 20 ns to better understand

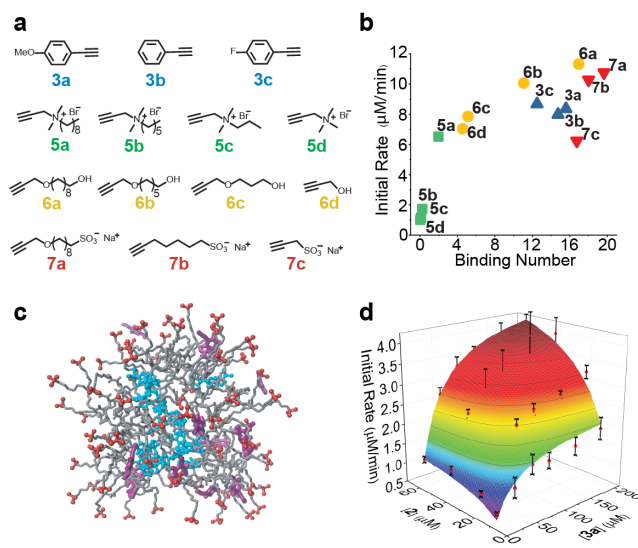


Figure 3. Uptake mode: CuAAC click reaction of small molecules. (a) Substrates with different charge species and hydrophobicity. (b) Initial rates of different substrates with the catalysis of Cu^I-SCNP-2 over their binding number during the simulation. (c) Snapshot of the substrate binding of SCNP-2 from MD simulation. The trimethyl ammonium structures were colored red, the catalytic centers were colored blue, other hydrophobic parts on SCNP-2 were colored grey and the substrate (**3a**) was colored purple. (d) Fitting of Cu^I-SCNP-2 kinetic data to a random-sequential two-substrate Bi-Bi enzyme kinetics equation fitting of Cu^I-SCNP-2 kinetics data. Reaction rates determined by fluorimeter with Cu^I-SCNP-2 (0.5 μM), **2** (10 - 60 μM), **3a** (10 - 200 μM), and NaAsc (2 mM) in PBS buffer (1x, pH = 7.4) at room temperature.

the nature of the macromolecular effect. The polymer exhibited a globular structure with a diameter of ca. 5.5 nm with a hydrophobic core and ammonium ions residing on the surface (Figure 3c). Identical MD simulations of SCNP-2 were performed but with alkyne substrates present; the average number of molecules bound during the last 10 ns was calculated. Not surprisingly, SCNP-2 exhibited a higher degree of occupancy with anionic and longer chain alkynes (Figures 3b and S9). A general correlation between the uptake and reactivity is observed and is consistent with enzyme-like activity. Experimental support for the encapsulation of alkyne **3a** by SCNP-2 was obtained using two-dimensional nuclear Overhauser spectroscopy (2D-NOESY) (Figure S8). The importance of substrate binding was also observed in the kinetic profile of Cu^I-SCNP-2. The rates of the CuAAC reaction of Cu^I-SCNP-2 with varying amounts of **2** and **3a** showed enzyme-like saturation kinetics in both alkyne and azide. The reaction rate surface could be fit to a two-substrate enzyme kinetics equation

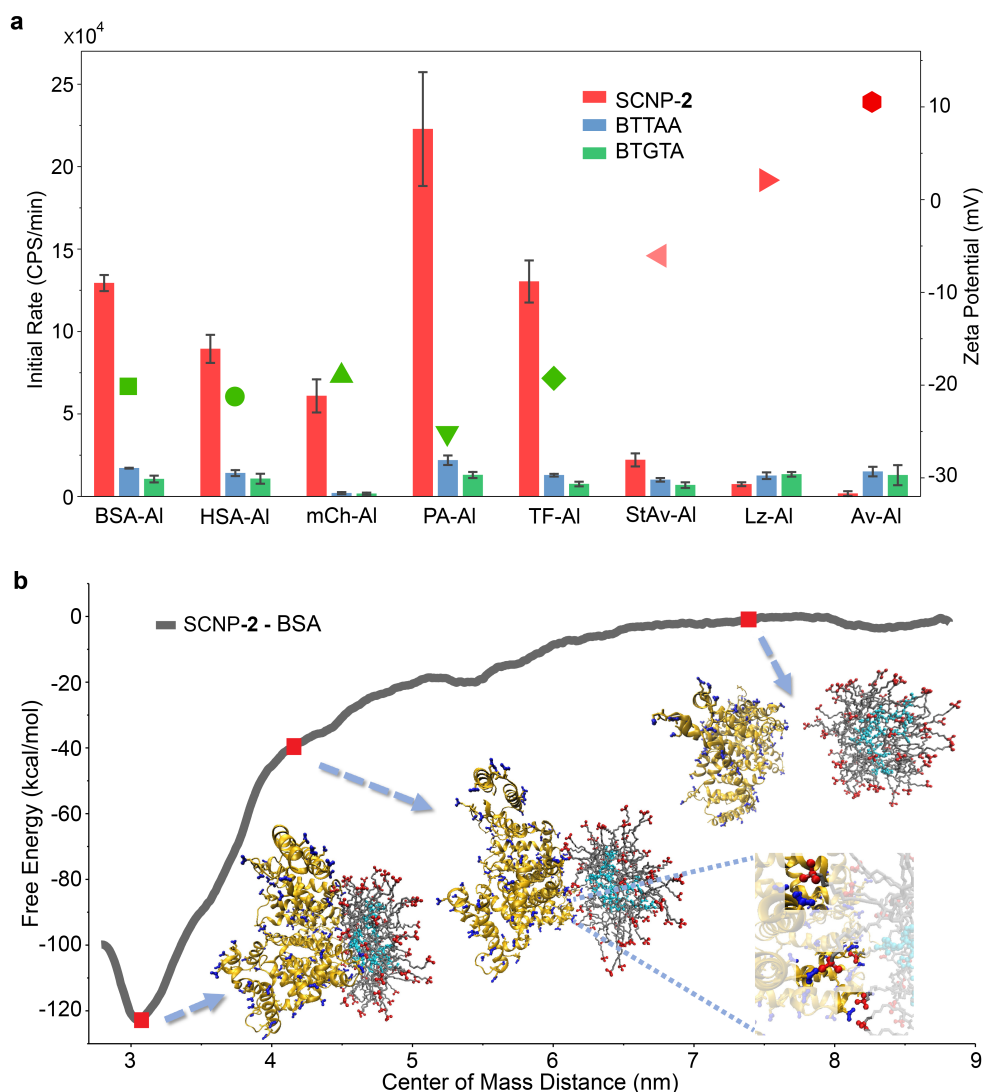


Figure 4. CuAAC reactions on proteins and simulation between Cu^I-SCNP-2 and BSA protein. (a) Initial rates for the modification of 2 μM of different proteins (for Lz-AI 5 μM) with Cu^I-SCNP-2 (2 μM) or BTTAA (20 μM), of **2** (40 μM) and sodium ascorbate (2 mM) in PBS buffer (1x, pH = 7.4) at room temperature. The error bars stand for the standard deviation of three independent experiments. Zeta potential of proteins in PBS buffer (1x, pH = 7.4). (b) MD simulation between a single SCNP-2 and BSA protein in PBS buffer (1x, pH = 7.4), and free energy was calculated from center of mass distance from 2.8 nm to 8.8 nm. The carboxylate groups on BSA protein were colored blue and the other parts were colored yellow. Snapshots were shown at 3.1 nm, 4.2 nm and 7.4 nm with a blow-up image at 4.2 nm showing the interactions

with random sequential Bi-Bi model (Figure 3d and Figure S7, see detail information under fluorogenic reaction with small molecules in the experimental section).²⁹

Attach Mode: CuAAC Click Reaction on Protein Substrates. Transition metal catalysts serve as important tools for modifying proteins, however, protein concentrations typically in the micromolar range require catalysts that are both highly active and biocompatible.³⁰⁻³⁵ Given the high activity of Cu^I-SCNP-2 in the CuAAC reaction, we sought to test its ability to operate on proteins. To this end, the surface lysine groups of several proteins were alkynylated with the NHS-ester of 4-pentynoic acid. Bovine serum albumin (BSA-AI), human serum albumin (HAS-AI), protein A (PA-AI), mCherry (mCh-AI), transferrin (TF-AI), and lysozyme (Lz-AI), were selected because of their diverse size, shape, and function. The average number of alkynes linked to each protein ranged from two (Lz-AI) to thirteen (BSA-AI and HAS-AI) and was determined by

MALDI-MS (Figure S11). Two additional proteins streptavidin (StAv-AI) and avidin (Av-AI) were also used, in this case the alkynes were added as biotinylated substrates (see Supporting Information for the structure).

All eight alkynylated proteins were clicked to coumarin azide **2** in PBS buffer, comparing the rate for catalysts Cu^I-SCNP-2, Cu^I-BTTAA and Cu^I-BTGTA at the same copper concentration (Figure 4a). An increase in fluorescence indicates both the rate and extent of coumarin azide **2** conjugation to the protein alkyne groups. In the case of BSA-AI, the reaction was further monitored by matrix-assisted laser desorption ionization (MALDI) mass spectrometry. Spectra taken before and after the CuAAC reaction of BSA-AI indicated nearly complete reaction of the alkyne groups (Figure S13). For five of the proteins (BSA-AI, HAS-AI, PA-AI, mCh-AI and TF-AI), the Cu^I-SCNP-2 catalyzed reaction was very fast with the increase in fluorescence plateauing at ca. 10 min (Figure S12). More

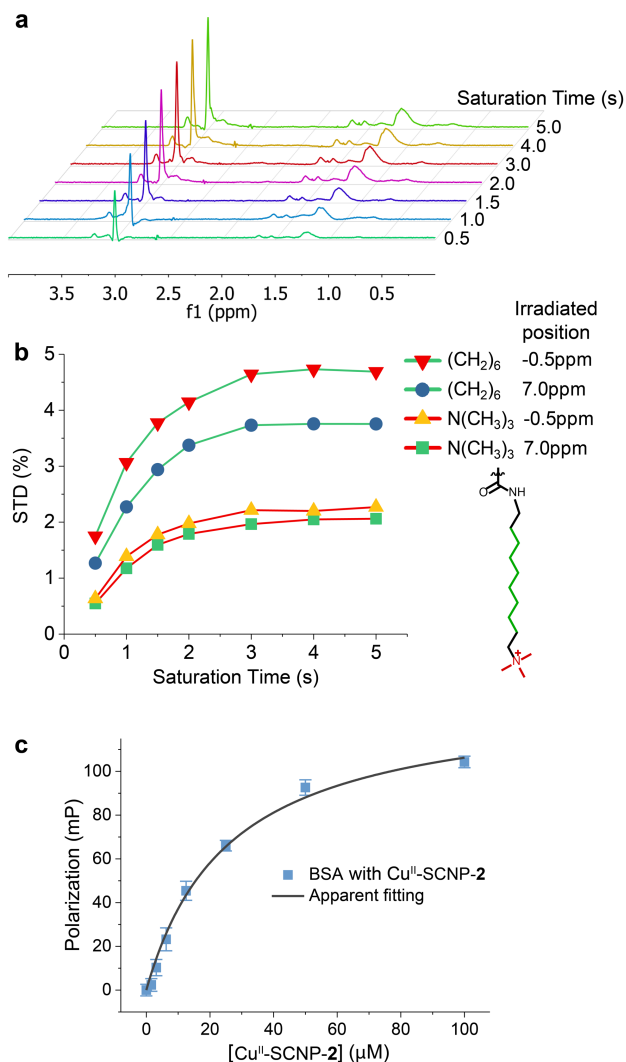


Figure 5. Experimental evidence of SCNP-protein interaction. (a) STD signals of Cu^{I} -SCNP-2 (100 μM) with different irradiation time on BSA (100 μM) at 7.0 ppm in deuterium PBS buffer (1x, pD = 7.4). (b) Percentage of STD signals of the trimethyl ammonium structure and hydrophobic chains on Cu^{I} -SCNP-2 (100 μM) or Cu^{I} -SCNP-3 (100 μM) with BSA (100 μM) protein in deuterium PBS buffer (1x, pD = 7.4) irradiated at 7.0 ppm. (c) Fluorescence polarization of fluorescein labeled BSA (2 μM) with different concentration of Cu^{I} -SCNP-2 in PBS buffer (1x, pH = 7.4). The error bars represent the standard deviation of three independent experiments.

importantly, the reaction rates were 10- to 26-times higher than for Cu^{I} -BTAA and Cu^{I} -BTGA (Figure 4a). However, StAv-Al proceeded only 2-3 times faster with Cu^{I} -SCNP-2 and for Av-Al and Lz-Al, the rates with Cu^{I} -BTAA and Cu^{I} -BTGA were faster.

The superior bioconjugation performance of Cu^{I} -SCNP-2 with the majority of the proteins was unexpected and suggested selective complexation of the proteins by the nanoparticle. This model involves a surface electrostatic complementarity, with accessible copper centers in the polymer able to couple the protein alkyne groups to coumarin azide **2**. Consistent with this model and the observed selectivity, the zeta potentials of the five highly reactive proteins (BSA-Al, HAS-Al, mCh-Al, PA-Al and TF-Al) ranged from -19 to -25 mV indicating anionic charged surfaces (Figure 4a). In contrast, StAv-Al had a nearly neutral surface, and Av-Al and Lz-Al exhibited a polycationic

surface. The measured zeta potentials are consistent with the reported isoelectric points (PI) of the proteins.

We prepared BTGA to evaluate the role of a single cationic guanidinium group on the catalysis, given its known ability to bind proteins. Cu^{I} -BTGA performs only slightly faster than Cu^{I} -BTAA suggesting the importance of multivalent binding by Cu^{I} -SCNP-2.³⁶ To obtain a more detailed picture of the multivalent surface complexation, which we refer to as “attach mode,” MD simulations were conducted with a single SCNP-2 and BSA. A non-equilibrium pulling calculation was performed over the center of mass distance (CMD) between the two macromolecules from 2.8 nm to 8.8 nm to provide a semi-quantitative estimate of their association free energy (Figure 4b). It was found that at a CMD of ca. 3.1 nm, the system showed the lowest free energy at -122 kcal/mol. At this distance, SCNP-2 was attached to BSA protein by a combination of apolar contacts and electrostatic interactions.

When the CMD was increased from 3.1 to 8.8 nm, the free energy of the system gradually increased as the hydrophobic regions of SCNP-2 detached from BSA protein (Movie S1). As shown in the inset in Figure 4b, several trimethylammonium-carboxylate ion pairs were found during this stage. This observation suggested that the SCNP-protein interaction may initially be facilitated by electrostatic interactions and further enhanced by subsequent contacts between the hydrophobic regions. At distances >7 nm, the nanoparticle became fully detached from the protein and the free energy reached a plateau. Despite the ten cross-links, the shape of SCNP-2 was not static, changing from globular when uncomplexed (CMD >7 nm) to an elongated shape that maximized the intermolecular contacts when bound to BSA (CMD = 3.1 nm). As a control, MD simulations were performed with avidin, a positively charged protein, and a significantly lower binding energy (-31 kcal/mol) was calculated (Figure S10).

The results from the protein conjugation studies and MD simulations prompted us to obtain experimental evidence for the SCNP-protein interaction. We previously studied the encapsulation of small molecules within SCNP-1¹⁸ by nuclear magnetic resonance saturation transfer difference (NMR STD) spectroscopy,³⁷ which uses the intermolecular nuclear Overhauser effect (NOE). The same technique was used here to examine the interaction between BSA and SCNP-2. The STD signals for peaks corresponding to the trimethyl ammonium groups and the hydrophobic alkyl chains on SCNP-2 were determined. As shown in Figure 5a and 5b, the STD signal for the alkyl side-chain and trimethylammonium groups of SCNP-2 increased with

increasing saturation time indicating its interaction with the protein, consistent with the MD simulations.

Fluorescence polarization experiments were conducted to estimate the strength of the SCNP-protein interaction. Thus, the polarization of fluorescein labelled BSA was measured with increasing concentration of SCNP-2. The apparent K_d calculated was 26 μM for SCNP-2 (Figure 5c), which is higher than the working concentration for the catalysis (2 μM). Only a very small degree of fluorescence polarization was observed at 2 μM suggesting a relatively weak and reversible SCNP-protein interaction under catalytic conditions, which is further supported by Förster resonance energy transfer (FRET) experiments (Figure S16). The weak binding did not result in aggregation as detected by DLS (Figure S15) nor any detectable change in protein structure as seen by the circular dichroism (CD) spectrum (Figure S17).

CuAAC Click Reaction on Cell Surfaces. Cell surface glycans are essential for cellular recognition, receptor signaling, and intracellular trafficking.³⁸ Given the high CuAAC activity observed with Cu^I-SCNP-2 and its ability to function effectively in bioconjugation, we examined the potential to perform catalysis on cell surface glycans. Thus, H460 cells were incubated with Ac4ManNAI or Ac4ManNAz separately to metabolically incorporate alkyne or azido groups into the cell surface glycans.³⁹ The alkyne-labelled cells were treated with coumarin azide **2** and either Cu^I-SCNP-2 (1 μM) or Cu^I-BTGTA (10 μM). An even more demanding labeling was examined by using the same two catalysts but treating the azide-labeled cells with alkynylated mCherry (mCh-Al). Cu^I-SCNP-2 again proved significantly more effective than Cu^I-BTGTA giving a strongly labeled cell membrane with coumarin azide **2** (Figure 6b) and mCh-Al (Figure 6d). Because the cell membrane and mCh-Al have a highly negative surface charge the cationic nanoparticle is able to bring them in proximity⁴⁰ allowing the copper centers to perform the CuAAC coupling. Indeed, this strategy significantly reduced the required amount of cytotoxic copper ([Cu^I] = 10 μM) so that no toxicity was observed (Figure S20).

CONCLUSION

Our results indicate that combining transition metal catalytic centers and polymeric scaffolds with substrate binding ability serves as a powerful method to increase catalyst efficiency. Cu^I-SCNP-2 functions analogously to enzymes by binding substrates in proximity to the metal center, thereby dramatically accelerating reaction rates at low substrate concentrations. The single-chain nanoparticle was also found to perform bioconjugation reactions to a range of protein substrates. We propose that these SCNPs function as supramolecular catalysts in two distinct ways. The first involves encapsulation involving an uptake mode for small molecules. The second was unexpected, an attach mode operating on protein substrates. In this mode a multivalent surface binding process overcomes what would otherwise be a sterically demanding reaction. Thus, the semi-flexible synthetic polymer adapts to the surface of the biomacromolecule and catalyzes the CuAAC reaction. The two proposed modes by which the copper SCNP functions represent limiting cases for small molecules and proteins and there will be a spectrum of mechanisms depending on the specific substrate.

The demonstration of these SCNPs as highly efficient catalysts for the “native” CuAAC reaction, suggest their utility in bioconjugation reactions. More broadly, the polymeric structure of SCNP loosely mimics the protein scaffold of metalloenzymes. Thus, the folded amphiphilic polymer selectively and reversibly binds substrates in aqueous buffer much like enzymes. Although well-defined binding pocket are lacking, the polymer increases the local concentration of substrate and the chance of collision with the metal site. As a result, enzyme-like saturation kinetics are observed. Obvious extensions to other catalytic reactions and even multi-step synthetic transformations are easy to envision and a current focus in our laboratory.

EXPERIMENTAL SECTION

Fluorogenic reaction with small molecules. The fluorogenic CuAAC click reactions were performed in a 0.7-mL fluorimeter cuvette. Catalyst ligand and CuSO₄ in a 1:1 ratio and NaAsc were dissolved in 0.5 mL of PBS buffer (1x, pH = 7.4) in the cuvette. DMSO stock solutions of substrates were added to give a final concentration of [NaAsc] = 2 mM and 2% (v/v) of DMSO. The click reaction of 3-azido-7-hydroxy-coumarin (**2**) forms compound **4** with restored fluorescence. The intensity was monitored using a fluorimeter in kinetics mode, measuring the fluorescence intensity every 10 s at $\lambda_{\text{em}} = 488$ nm with excitation at $\lambda_{\text{ex}} = 410$ nm. The initial rate was determined using the following procedure: Approximately 20-30 s after the start of the reaction, where the fluorescence signals start to increase linearly over time, the slope of this linear part (5-15 data

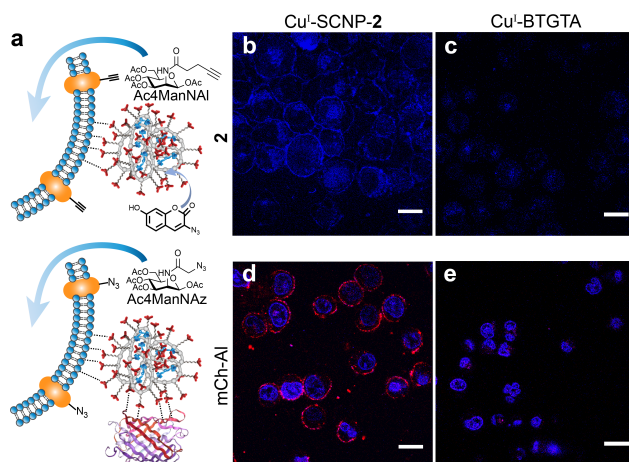


Figure 6. Reactions on cell surface glycans. (a) Illustration of metabolic labelling of cell surface glycan by using a mannose derivative with an azido or alkyne group, and Cu^I-SCNP-2 mediated reactions on cell membrane. (b) and (c) Confocal images of alkyne-labelled H460 cell treated with Cu^I-SCNP-2 (1 μM) (b) or Cu^I-BTGTA (10 μM) (c), **2** (100 μM) and sodium ascorbate (2 mM) in PBS buffer (1x, pH = 7.4) for 30 min. (d) and (e) Confocal images of azide-labelled H460 cell treated with Cu^I-SCNP-2 (1 μM) (d) or Cu^I-BTGTA (10 μM) (e), mCh-Al (1 μM) and sodium ascorbate (2 mM) in PBS buffer (1x, pH = 7.4) for 30 min. Nucleus were stained with Hoechst for (d) and (e). Scale bar = 20 μm .

points) was calculated in counts per second (CPS) increase per minute. For the reaction between **2** and **3a**, the slope was calculated into the initial reaction rate in “ $\mu\text{M}/\text{min}$ ” from the observed fluorescence intensity using pure **4** as

the standard. The initial reaction rates for the other 13 alkyne substrates were calculated based on the assumption that the reactions reach 100% conversion, and the plateaued fluorescent signal corresponds to 20 μM of the product. The fluorogenic CuAAC click reactions on protein were performed using a similar procedure with the initial rate presented directly as "CPS/min." For enzyme-like kinetics fitting experiment, the initial reaction rates of the reactions between **2** (10, 20, 40, 60 μM) and **3a** (10, 40, 70, 150, 200 μM) with catalysis by Cu^I-SCNP-2 (0.5 μM) were measured. The initial reaction rates were fit to a random sequential two-substrates enzyme kinetics equation:

Protein functionalization with alkyne groups. In a 1.5-mL centrifuge tube, protein (BSA, HSA, mCherry, protein A, or transferrin) was dissolved in PBS buffer (1x, pH = 7.4, 1 mL) at a concentration of 100 μM . Then, 2,5-dioxopyrrolidin-1-yl pent-4-ynoate (0.2 mg) in DMSO (4 μL) was added to the protein solution. The mixture was gently shaken for 6 h at room temperature and small organic compounds were removed using an Amicon tube with 10 kDa cut-off. For lysozyme, due to the smaller molecular weight, it was dissolved in PBS buffer (1x, pH = 7.4, 1 mL) at the concentration of 550 μM and 2,5-dioxopyrrolidin-1-yl pent-4-ynoate (0.2 mg) in DMSO (4 μL) was added. The mixture was gently shaken for 6 h at room temperature and purified by an Amicon tube with 3 kDa cutoff. The molecular weight of the protein before and after functionalization were determined using matrix-assisted laser desorption/ionization (MALDI) mass spectrometry and the average number of alkynes were determined by the molecular weight increases. Functionalized proteins are referred to as BSA-Al, HSA-Al, mCh-Al, PA-Al, TF-Al and Lz-Al. For functionalizing streptavidin and avidin with three alkyne groups, each protein was dissolved in PBS buffer (1x, pH = 7.4, 1 mL) at the concentration of 100 μM . Biotin-PEG4-alkyne was added to reach the concentration of 300 μM (3 equivalents). The mixture was gently shaken for 10 min and used without further purification. The noncovalently functionalized streptavidin and avidin are referred to as StAv-Al and Av-Al.

2D-NOESY experiments. Cu^{II}-SCNP-2 was dissolved in D₂O at the concentration of 100 μM and the small molecules were added as a 200 mM DMSO-*d*₆ stock solution to reach a final concentration of 3 mM (30 equivalents). 2D-NOESY spectra were collected using a water suppression 2D-NOESY method on a Bruker CB500. Spectra were processed with base line correction and phase correction by using MestReNova (v. 8.1). Substrate **3a** showed relatively strong intermolecular NOE signals between its aromatic signals and the SCNP-2 alkyl signals at 1.2 ppm, and little cross-peak NOE signals were observed from the other protons on SCNP-2. Due to signal overlap between the charged alkyne substrates (group **5** and **7**) and SCNP-2, the intermolecular NOE signals between SCNP-2 with charged molecule were studied with sodium benzenesulfonate and benzyl trimethylammonium chloride. Using the above condition, the intermolecular NOE signals were observed from both alkyl region (1.2 ppm) and trimethyl ammonium (3.0 ppm) regions on SCNP-2 to benzenesulfonate, suggesting both electrostatic interactions and hydrophobic interactions are involved in binding anionic small molecules. Almost no NOE cross-peaks were observed between benzyl

trimethylammonium chloride and SCNP-2, suggesting weak binding of cationic molecules.

Saturation Transfer Difference (STD) experiment. BSA with Cu^{II}-SCNP-2 or Cu^{II}-SCNP-3 were dissolved in deuterium oxide PBS buffer (1x, pD = 7.4) to reach a concentration of 100 μM for both protein and nanoparticle. STD spectra were collected using a water suppression STD method on a VNS750 spectrometer with the bio-pack software. During the saturation period, the aromatic region of BSA was irradiated at 7 ppm or -0.5 ppm, with the irradiation time ranging from 0.5 s to 5 s. To minimize intramolecular signals from BSA, a 15 ms relaxation T₂ filter was applied during data acquisition. Spectra were

$$v = \frac{V_{\max}[A][B]}{K_S^A K^{AB} + K^{AB}[A] + K^{BA}[B] + [A][B]}$$

processed by MestReNova (v. 8.1), and the STD effect intensity was calculated for the trimethyl ammonium peak at 3.0 ppm and alkyl chain peak at 1.2 ppm through the equation: STD = (I₀ - I_{sat})/I₀.

Fluorescence Polarization. Fluorescein labelled BSA protein was dissolved in PBS buffer (1x, pH = 7.4) at the concentration of 2 μM with the concentration of Cu^{II}-SCNP-2 ranging from 0 to 100 μM . The solutions were transferred to a black 384-well plate, and 50 μL of the solution was added to each well. The fluorescence polarization of solutions in each well was measured on an Analyst HT plate reader with the setup on fluorescein. The data was processed and fit using OriginPro2017.

Cell study. In a 6-wells plate, 30000 of H460 cells were added in 3 mL of DMEM media (10% FBS) containing Ac₄ManNAz (25 μM) or Ac₄ManNAL (25 μM) to each well with a glass slide. The cells were incubated at 37 °C with 5% CO₂ for 72 h for metabolic incorporation. Cell media was removed, and each well was washed three times with 3 mL of PBS buffer (1x, pH = 7.4). DMEM media (10% FBS) without Man-Al (3 mL) was added to each well and incubated for 1 h to deplete free Ac₄ManNAz or Ac₄ManNAL. Cell media was removed and each well was washed three times with 3 mL of PBS buffer (1x, pH = 7.4). For each well, 5 mL of PBS buffer (1x, pH = 7.4) with/without Cu^I-SCNP-2 (1 μM), Cu^I-BTGTA (10 μM) or Cu^I-BTAA (10 μM), **2** (100 μM) or mCh-Al (1 μM) and sodium ascorbate (2 mM) was added. The cells were incubated at 37 °C with 5% CO₂ for 0.5 h for the CuAAC reaction. The solutions were removed and each well was washed three times with 3 mL of PBS buffer (1x, pH = 7.4). For the cellular click reactions performed with mCh-Al, the cell nucleus was stained with Hoechst 33342 (8 μM in PBS buffer) for 2-3 min and subsequently washed three times with 3 mL of PBS buffer. The samples were imaged using a Leica SP8 UV/Visible Laser Confocal Microscope (excitation = 405 nm and 561 nm, blue channel: emission = 450-500 nm on the PMTs detector, red channel: 600-650 nm on the high-sensitivity GaAsP HyD detectors).

ASSOCIATED CONTENT

Supporting Information.

The Supporting Information is available free of charge on the ACS Publications website at DOI:

General experimental procedures and detailed synthetic procedures and characterization data for small molecules

and polymers, and additional kinetic data along with details of the computational methods (PDF)

AUTHOR INFORMATION

Corresponding Author

* E-mail: sczimmer@illinois.edu.

ORCID

Junfeng Chen: 0000-0002-7100-0839

Jiang Wang: 0000-0002-3871-598X

Ke Li: 0000-0003-3851-7710

Yuhan Wang: 0000-0001-6807-3968

Martin Gruebele: 0000-0001-9291-8123

Andrew L. Ferguson: 0000-0002-8829-9726

Steven C. Zimmerman: 0000-0002-5333-3437

Notes

The authors declare no competing financial interest.

ACKNOWLEDGMENT

This work was supported by the National Science Foundation (NSF CHE-1709718, DMS-1841810, and MCB-1803786) and the National Institutes of Health (R01AR058361).

REFERENCES

- (1) Bai, Y.; Chen, J.; Zimmerman, S.C. Designed transition metal catalysts for intracellular organic synthesis. *Chem. Soc. Rev.* **2018**, *47*, 1811-1821.
- (2) Yang, M.; Li, J.; Chen, P. R. Transition metal-mediated bioorthogonal protein chemistry in living cells. *Chem. Soc. Rev.* **2014**, *43*, 6511-6526.
- (3) Martínez-Calvo, M.; Mascareñas, J. L. Organometallic catalysis in biological media and living settings. *Coord. Chem. Rev.* **2018**, *359*, 57-79.
- (4) Vinogradova, E. V.; Zhang, C.; Spokoyny, A. M.; Pentelute, B. L.; Buchwald, S. L. Organometallic palladium reagents for cysteine bioconjugation. *Nature* **2015**, *526*, 687-691.
- (5) Jiang, H.; López-Aguilar, A.; Meng, L.; Gao, Z.; Liu, Y.; Tian, X.; Yu, G.; Ovrzyn, B.; Moremen, K. W.; Wu, P. Modulating cell-surface receptor signaling and ion channel functions by in situ glycan editing. *Angew. Chem. Int. Ed.* **2018**, *57*, 967-971.
- (6) Coverdale, J. P. C.; Romero-Canelón, I.; Scanchez-Cano, C.; Clarkson, G. J.; Habtemariam, A.; Wills, M.; Sadler, P. J. Asymmetric transfer hydrogenation by synthetic catalysts in cancer cells. *Nat. Chem.* **2018**, *10*, 347-354.
- (7) Rebelein, J. G.; Ward, T. R. In vivo catalyzed new-to-nature reactions. *Curr. Opin. Biotechnol.* **2018**, *53*, 106-114.
- (8) Yu, F.; Cangelosi, V. M.; Zastrow, M. L.; Tegoni, M.; Plegaria, J. S.; Tebo, A. G.; Mocny, C. S.; Ruckthong, L.; Qayyum, H.; Pecoraro, V. L. Protein design: toward functional metalloenzymes. *Chem. Rev.* **2014**, *114*, 3495-3578.
- (9) Cole, J. P.; Hanlon, A. M.; Rodriguez, K. J.; Berda, E. B. Protein-like structure and activity in synthetic polymers. *J. Polym. Sci. Part A: Polym. Chem.* **2017**, *55*, 191-206.
- (10) Rothfuss, H.; Knofel, N. D.; Roesky, P. W.; Barner-Kowollik, C. Single-chain nanoparticles as catalytic nanoreactors. *J. Am. Chem. Soc.* **2018**, *140*, 5875-5881.
- (11) Mavila, S.; Eivgi, O.; Berkovich, I.; Lemcoff, N. G. Intramolecular cross-linking methodologies for the synthesis of polymer nanoparticles. *Chem. Rev.* **2016**, *116*, 878-961.

(12) Rubio-Cervilla, J.; González, E.; Pomposo, J. A. Advances in single-chain nanoparticles for catalysis applications. *Nanomaterials* **2017**, *7*, 341-360.

(13) Pomposo, J. A., Ed. *Single-Chain polymer nanoparticles: synthesis, characterization, simulations, and applications*; John Wiley & Sons, 2017.

(14) Bai, Y.; Xing, H.; Vincil, G. A.; Lee, J.; Henderson, E. J.; Lu, Y.; Lemcoff, N. G.; Zimmerman, S. C. Practical synthesis of water-soluble organic nanoparticles with a single reactive group and a functional carrier scaffold. *Chem. Sci.* **2014**, *5*, 2862-2868.

(15) Bai, Y.; Xing, H.; Wu, P.; Feng, X.; Hwang, K.; Lee, J. M.; Phang, X. Y.; Lu, Y.; Zimmerman, S. C. Chemical control over cellular uptake of organic nanoparticles by fine tuning surface functional groups. *ACS Nano* **2015**, *9*, 10227-10236.

(16) Bai, Y.; Feng, X.; Xing, H.; Xu, Y.; Kim, B. K.; Baig, N.; Zhou, T.; Gewirth, A. A.; Lu, Y.; Oldfield, E.; Zimmerman, S. C. A highly efficient single-chain metal-organic nanoparticle catalyst for alkyne-azide "click" reactions in water and in cells. *J. Am. Chem. Soc.* **2016**, *138*, 11077-11080.

(17) Liu, Y.; Pujals, S.; Stals, P. J. M.; Paulöhr, T.; Presolski, S. I.; Meijer, E. W.; Albertazzi, L.; Palmans, A. R. A. Catalytically active single-chain polymeric nanoparticles: exploring their functions in complex biological media. *J. Am. Chem. Soc.* **2018**, *140*, 3423-3433.

(18) Chen, J.; Wang, J.; Bai, Y.; Ke, L.; Garcia, E. S.; Ferguson, A. L.; Zimmerman, S. C. Enzyme-like click catalysis by a copper-containing single-chain nanoparticle. *J. Am. Chem. Soc.* **2018**, *140*, 13695-13702.

(19) Huerta, E.; Stals, P. J. M.; Meijer, E. W.; Palmans, A. R. A. Consequences of folding a water-soluble polymer around an organocatalyst. *Angew. Chem. Int. Ed.* **2013**, *52*, 2906-2910.

(20) Rostovtsev, V. V.; Green, L. G.; Fokin, V. V.; Sharpless, K. B. A Stepwise Huisgen cycloaddition process: copper(I)-catalyzed regioselective "ligation" of azides and terminal alkynes. *Angew. Chem.* **2002**, *114*, 2708-2711.

(21) Rodionov, V. O.; Presolski, S. I.; Gardinier, S.; Lim, Y. H.; Finn, M. G. Benzimidazole and related ligands for Cu-catalyzed azide-alkyne cycloaddition. *J. Am. Chem. Soc.* **2007**, *129*, 12696-12704.

(22) Besanceney-Webler, C.; Jiang, H.; Zheng, T.; Feng, L.; Soriano del Arno, D.; Wang, W.; Klivansky, L. M.; Marlow, F. L.; Liu, Y.; Wu, P. Increasing the efficacy of bioorthogonal click reactions for bioconjugation: a comparative study. *Angew. Chem. Int. Ed.* **2011**, *50*, 8051-8056 (2011).

(23) Ovrzyn, B.; Li, J.; Hong, S.; Wu, P. Visualizing glycans on single cells and tissues—Visualizing glycans on single cells and tissues. *Curr. Opin. Chem. Biol.* **2017**, *39*, 39-45.

(24) Frisch, H.; Menzel, J. P.; Bloesser, F. R.; Marschner, D. E.; Mundsinger, K.; Barner-Kowollik, C. Photochemistry in confined environments for single-chain nanoparticle design. *J. Am. Chem. Soc.* **2018**, *140*, 9551-9557.

(25) Sivakumar, K.; Xie, F.; Cash, B. M.; Long, S.; Barnhill, H. N.; Wang, Q. A Fluorogenic 1,3-dipolar cycloaddition reaction of 3-azidocoumarins and acetylenes. *Org. Lett.* **2004**, *6*, 4603-4606.

(26) Chan, T. R.; Hilgraf, R.; Sharpless, K. B.; Fokin, V. V. Polytriazoles as copper(I)-stabilizing ligands in catalysis. *Org. Lett.* **2004**, *6*, 2853-2855.

(27) Artar, M.; Souren, E. R. J.; Terashima, T.; Meijer, E. W.; Palmans, A. R. A. Single chain polymeric nanoparticles as selective hydrophobic reaction spaces in water. *ACS Macro Lett.* **2015**, *4*, 1099-1103.

- (28) Liu, Y.; Turunen, P.; de Waal, B. F. M.; Blank, K. G.; Rowan, A. E.; Palmans, A. R. A.; Meijer, E. W. Catalytic single-chain polymeric nanoparticles at work: from ensemble towards single-particle kinetics. *Mol. Syst. Des. Eng.* **2018**, *3*, 609-618
- (29) Ivanetich, K. M.; Goold, R. D. A rapid equilibrium random sequential bi-bi mechanism for human placental glutathione S-transferase. *Biochim. Biophys. Acta, Protein Struct. Mol. Enzymol.* **1989**, *998*, 7-13.
- (30) Antos, J. M.; Francis, M. B. Transition metal catalyzed methods for site-selective protein modification. *Curr. Opin. Chem. Biol.* **2006**, *10*, 253-262.
- (31) Spicer, C. D.; Davis, B. G. Selective chemical protein modification. *Nat. Commun.* **2014**, *5*, 4740-4753.
- (32) Jbara, M.; Maity, S. K.; Brik, A. Palladium in the chemical synthesis and modification of proteins. *Angew. Chem. Int. Ed.* **2017**, *56*, 10644-10655.
- (33) Koniev, O.; Wagner, A. Developments and recent advancements in the field of endogenous amino acid selective bond forming reactions for bioconjugation. *Chem. Soc. Rev.* **2015**, *44*, 5495-5551.
- (34) Boutureira, O.; Bernardes, G. J. L. Advances in chemical protein modification. *Chem. Rev.* **2015**, *115*, 2174-2195.
- (35) Takaoka, Y.; Ojida, A.; Hamachi, I. Protein organic chemistry and applications for labeling and engineering in live-cell systems. *Angew. Chem. Int. Ed.* **2013**, *52*, 4088-4106.
- (36) Mogaki, R.; Hashim, P. K.; Okuro, K.; Aida, T. Guanidinium-based "molecular glues" for modulation of biomolecular functions. *Chem. Soc. Rev.* **2017**, *46*, 6480-6491.
- (37) Mayer, M.; Meyer, B. Characterization of ligand binding by saturation transfer difference NMR spectroscopy. *Angew. Chem. Int. Ed.* **1999**, *38*, 1784-1788.
- (38) Ohtsubo, K.; Marth, J. D. Glycosylation in cellular mechanisms of health and disease. *Cell* **2006**, *126*, 855-867.
- (39) Prescher, J. A.; Dube, D. H.; Bertozzi, C.R. Chemical remodelling of cell surfaces in living animals, *Nature* **2004**, *430*, 873-877.
- (40) Verma, A.; Stellacci, F. Effect of surface properties on nanoparticle-cell interactions. *Small* **2010**, *6*, 12-21.

Table of contents (TOC) graphic

